International Journal of Control, Automation and Systems 16(6) (2018) 2915-2923
http://dx.doi.org/10.1007/s12555-017-0486-3
ISSN:1598-6446 eISSN:2005-4092
http://www.springer.com/12555

Safety-enhanced Collaborative Framework for Tele-operated Minimally Invasive Surgery Using a 7-DoF Torque-controlled Robot

Hang Su*, Juan Sandoval, Pierre Vieyres, Gérard Poisson, Giancarlo Ferrigno, and Elena De Momi

Abstract: In this paper, a safety-enhanced collaborative control framework is proposed for tele-operated minimally invasive surgery (MIS) using a redundant 7-DoF serial robot. The redundant manipulators offer a safe physical collaborative flexible workspace for nurse or surgeon (assisting physicians, patient support) undergoing surgery. The novel framework integrates a Cartesian compliance control strategy to guarantee that the tele-operated surgical tool always goes through the trocar position, and a safety-enhanced null-space collaborative strategy to constrain the swivel motion in an assumed safe range. Two event-based operative procedures (hands-on motion and tele-operation) are performed in torque level to achieve the whole surgical task. Finally, experimental studies with virtual surgical tasks were conducted to validate the effectiveness of the proposed framework, using the KUKA LWR 4+ robot and Sigma 7 master device. It provided an online flexible and safe collaborative way without degradation of the quality of the surgical task.

Keywords: Minimally invasive surgery, redundant robot, safe collaborative null-space strategy, surgical robot tele-operation.

1. INTRODUCTION

During the past decades, the development of surgical robot systems for Minimally Invasive Surgery(MIS) has been significantly motivated by the rapid advancements in computing and sensor technologies. In the tele-operated MIS, surgical robots show advantages in safe and flexible manipulation [1], augmenting the ability of the surgeons. The commercially available tele-operated surgical robots involves da Vinci Surgical System manufactured by Intuitive Surgical, Inc., offer greater surgical precision, increased range of motion, improved dexterity, and enhanced visualization for the surgeons [2]. Inspired by the aforementioned advantages, various studies have been proposed with novel mechanical design [3,4] or advanced control algorithm [5,6] for the tele-operated surgical systems.

For all the tele-operated minimally invasive robotic systems, the operations of the instrument should always be performed through small incisions on the patient's body, which is commonly known as the Remote Center of Motion (RCM) constraint [7]. Tele-operated serial redundant manipulators can also serve as the surgical arms to effectively combine the surgical task and the RCM constraint [8,9]. Except for achieving the tele-operated surgical tasks with tool-tip, its kinematic redundancy can be exploited to accomplish additional tasks, for example, avoiding kinematic constraint [10], optimizing manipulability [11]. An interesting way to exploit the kinematic redundancy is to provide flexible workspace for human nurse or surgeon (assisting physicians, patient support) in the sharing workspace, which presupposes effective use of the robot. In the proposed scenario, the pose of the tool tip is controlled to achieve the main surgical operation. The redundancy can be utilized to work in a collaborative way to avoid collision in the workspace. For example, during the tele-operation control of the surgical robot, if the human nurse want do patient supporting, scraping, but the robot arm take the workspace. It is impossible to stop the ongoing surgery and move the robot arm. Using camera or 3-D sensor to avoid the collision [12] in a dynamic environment is also not safe and cannot acquired the trust of the patient. A compliant behavior is one powerful method to avoid unknown obstacles in such unknown environment for human-robot interaction, because the exact sensing of the manipulator configuration against the environment in

Manuscript received August 14, 2017; revised May 6, 2018; accepted July 12, 2018. Recommended by Associate Editor Sukho Park under the direction of Editor Hamid Reza Karimi. This work is supported by the Department of Electronics, Information and Bioengineering of the Politecnico di Milano, China Scholarship Council and French Ministry of Research.

Hang Su, Giancarlo Ferrigno and Elena De Momi are with the Department of Electronics, Information and Bioengineering, Politecnico di Milano, 20133, Milan, Italy (e-mails: {hang.su, giancarlo.ferrigno, elena.demomi}@polimi.it). Juan Sandoval is with Department of GMSC, Pprime Institute CNRS, ENSMA, University of Poitiers, UPR 3346, France (e-mail: juan.sebastian.sandoval.arevalo@univ-poitiers.fr). Pierre Vieyres and Gérard Poisson are with PRISME Laboratory, University of Orleans, INSA CVL, France (e-mails: {pierre.vieyres, gerard.poisson}@univ-orleans.fr).
* Corresponding author.

the operating room is really difficult. When there is a collision in the shared workspace between the human and the robot, the human can move the robot arm by hand. Furthermore, it should also avoid dangerous area existing in the robot's workspace. It is dangerous to move the robot arm near the kinematic limitation area or in unexpected area without any constraint, leading to a breakdown of the undergoing surgery. [12, 13] Therefore, the kinematic redundancy of the tele-operated robotic arm could be controlled in a safe collaborative way, also respecting the special surgery scene to avoid collision with human staff or other medical devices, without a degradation of the quality of the surgical task or a damage on the running system. In this paper, we propose a safety-enhanced collaborative control framework for tele-operated MIS, providing flexible and safe solution for the robot and the medical staff sharing the same workspace. It includes two main parts: Cartesian compliance strategy and constrained null-space compliance strategy. The implemented Cartesian compliance strategy involves online trajectory planning to avoid violation of the RCM constraint. The constrained null-space compliance strategy is proposed to restrict the collaborative swivel motion range, either by the feasible kinematic solution calculated online or by limitations due to the workspace scene. Moreover, Two event-based operative procedures (hands-on motion and tele-operation) are switched to each other online to achieve the whole surgical task [14]. A virtual reality interface is developed to validate the proposed strategy and visualize the whole operative procedure of the tasks online.

The paper is organized as follows: the dynamic model and kinematic model of the redundant manipulator is described in Section 2. In Section 3, we present the system description of the proposed tele-operated MIS system. Section 4 and Section 5 explain the methodology and experimental evaluation. Finally, in the last section we provide discussions and conclusions about the proposed control framework.

2. MODELING OF THE MANIPULATOR

2.1. Dynamic model

The dynamic model of a n-DoF serial manipulator in the Lagrangian formulation is expressed as:

$$\boldsymbol{M}(\boldsymbol{q})\ddot{\boldsymbol{q}}+\boldsymbol{C}(\boldsymbol{q},\dot{\boldsymbol{q}})+\boldsymbol{g}(\boldsymbol{q})=\boldsymbol{\tau_C}-\boldsymbol{\tau_{EXT}}, \tag{1}$$

where $\boldsymbol{q}\in R^n$ is the joint position, $\boldsymbol{M}(\boldsymbol{q})\in R^{n\times n}$ is the inertia matrix, $\boldsymbol{C}(\boldsymbol{q},\dot{\boldsymbol{q}})\in R^n$ is a matrix representing the Coriolis and Centrifugal effects, and $\boldsymbol{g}(\boldsymbol{q})\in R^n$ is the vector of gravity torques [15, 16]. The torque vectors $\boldsymbol{\tau_C}\in R^n$ and $\boldsymbol{\tau_{EXT}}\in R^n$ represent the control torques and the external torques vectors, respectively.

In order to perform the surgical task, the proposed controller introduces the desired torque term $\boldsymbol{\tau_d}\in R^n$, corresponding to the desired robot control tasks. Assuming that the robot uses external torque sensors to provide $\boldsymbol{\tau_{EXT}}$, and using the estimated compensation torques [17] $\hat{\boldsymbol{C}}(\boldsymbol{q},\dot{\boldsymbol{q}})\in R^n$ and $\hat{\boldsymbol{g}}(\boldsymbol{q})\in R^n$, the control torque solution can be defined as follows:

$$\boldsymbol{\tau_C}=\boldsymbol{\tau_d}+\hat{\boldsymbol{C}}(\boldsymbol{q},\dot{\boldsymbol{q}})+\hat{\boldsymbol{g}}(\boldsymbol{q})+\boldsymbol{\tau_{EXT}}. \tag{2}$$

For simplification, we assume that the surgical robot is far away from its singularity and the pseudoinverse of $\boldsymbol{J}\in R^{n\times n}$ exists.

Assumption 1: The time-varying disturbances $\boldsymbol{\tau_e}\in R^n$ from physical interaction between the tool and the abdominal wall are continuous in time and bounded, i.e.,

$$\exists\beta\in R, \|\boldsymbol{\tau_e}\|\leq\beta, \forall t\geq 0. \tag{3}$$

To achieve the m-DoF desired end-effector pose $\boldsymbol{X_d}\in R^m$ for the surgical tasks, one Cartesian compliance control term $\boldsymbol{\tau_T}\in R^n$ is defined based on the potential function of a virtual spring and a damping term, as used in [18], given by:

$$\boldsymbol{\tau_T}=\boldsymbol{J^T F_T}=\boldsymbol{J^T}((\frac{\partial \boldsymbol{V}(\boldsymbol{q})}{\partial \boldsymbol{X}})^T-\boldsymbol{D_x}\dot{\boldsymbol{X}}), \tag{4}$$

where $\boldsymbol{D_x}\in R^{m\times m}$ is the diagonal damping matrix, the virtual potential function $\boldsymbol{V}(\boldsymbol{q})$ is defined based on the difference between the desired and the actual Cartesian trajectory $\tilde{\boldsymbol{X}}(\boldsymbol{q})=\boldsymbol{X_d}-\boldsymbol{X}(\boldsymbol{q})$, as follows:

$$\boldsymbol{V}(\boldsymbol{q})=\frac{1}{2}\tilde{\boldsymbol{X}}(\boldsymbol{q})^T\boldsymbol{K_x}\tilde{\boldsymbol{X}}(\boldsymbol{q}), \tag{5}$$

where $\boldsymbol{X}(\boldsymbol{q})$ is the actual target pose calculated from forward kinematic function, $\boldsymbol{K_x}\in R^{m\times m}$ is the diagonal stiffness matrix.

Property 2.1: The inertia matrix $\boldsymbol{M}(\boldsymbol{q})$ is symmetric and positive, which is also bounded as

$$\lambda_1\|\boldsymbol{A}\|\leq\boldsymbol{A^T M}(\boldsymbol{q})\boldsymbol{A}\leq\lambda_2\|\boldsymbol{A}\|, \forall\boldsymbol{A},\boldsymbol{q}\in R^n \tag{6}$$

where λ_1 and λ_2 are positive constants.

Property 1: The matrix $\boldsymbol{C}(\boldsymbol{q},\dot{\boldsymbol{q}})$ and the time derivative of the inertia matrix $\boldsymbol{M}(\boldsymbol{q})$ satisfy

$$\boldsymbol{A}^T\dot{\boldsymbol{M}}(\boldsymbol{q})-2\boldsymbol{C}(\boldsymbol{q},\dot{\boldsymbol{q}})]\boldsymbol{A}=0, \forall\boldsymbol{A},\boldsymbol{q},\dot{\boldsymbol{q}}\in R^n. \tag{7}$$

2.2. Swivel motion of the robot arm

In the case of a 7-DoF serial robot, the degree of redundancy $r=n-m=7-6=1$ can be easily represented as a swivel angle ψ [13] shown in Fig. 1. As it is shown in the figure, O is the vertical intersection of OE and SW. The swivel angle is defined by the angle between the reference plane (BSW) and the actual arm plane (SEW). The swivel angle can be calculated

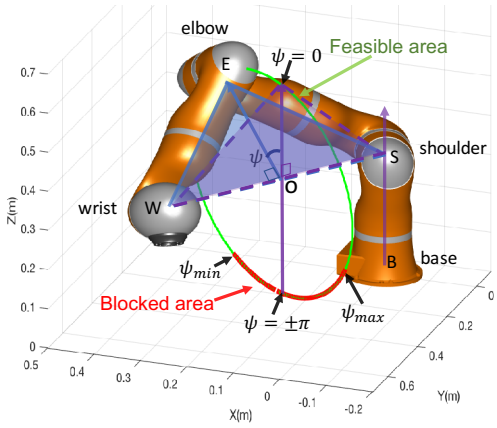

Fig. 1. Redundancy swivel solution.

by: $\psi = sgn((\vec{BS}\times\vec{SE})\cdot\vec{SW})\arccos(\frac{(\vec{BS}\times\vec{SW})(\vec{SE}\times\vec{EW})}{||\vec{BS}\times\vec{SW}||||\vec{SE}\times\vec{EW}||})$, Its ideal swivel range is defined as $[-\pi,\pi]$ including green part (feasible areas $[\psi_{min},\psi_{max}]$) and red part (blocked areas $[-\pi,\psi_{min})$ and $(\psi_{max},\pi]$). The reason for existing blocked area is joint limitations. It means when there is a fixed 6-DoF target pose, the swivel angle of the robot arm can still be freely to move around the axis $\hat{SW}$ defined between the robot's shoulder and elbow. However, the swivel motion range is constrained by the joint kinematic limitations [13]. Moreover, even if the ideal range of ψ is $[-\pi,\pi]$, the feasible swivel range is constrained with joint limitations. The optimal algorithm is adopted to calculate the corresponding feasible swivel range $[\psi_{min},\psi_{max}]$ based on the kinematic limitations in [13].

3. SYSTEM DESCRIPTION

An overview of the developed tele-operated surgery control system is shown in Fig. 2. The system includes a KUKA LWR 4+ redundant robot as the surgical robot, a SIGMA 7 master device (Force Dimension, Switzerland) as the master, a foot-switch pedal, a 720p webcam (30 fps) providing online visual feedback of task execution, an ArUco marker board around 21.0 cm × 29.7 cm, for establishment of the visual surgical task, a desktop with a 2.66GHZ Xeon 5150 CPU (Intel, Corp.) and 16GB RAM running Ubuntu 12.04 as a server for ROS communication. For the real-time control, a desktop with a 3.6 GHz Core i7-4790 CPU (Intel, Corp.) and 16GB RAM running a real-time patched Linux kernel (Kernel 3.5.7 patched with Xenomai 2.6.2.) is used as the control computer. Moreover, a laptop with a 2.66 GHz Core P9600 CPU and 8 GB RAM running a generic Linux kernel (3.19.0) is used for vision applications. This robot is torque-controlled with Fast Research Interface (FRI) at high rates of up to 1 kHz [17], allowing to implement compliant control strategies. Moreover, each joint includes a torque sensor to measure the external forces applied to the

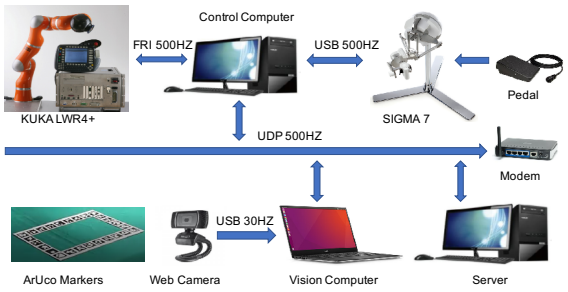

Fig. 2. The tele-operated surgical robot control system.

robot. The master device and pedal are working in incremental way for tele-operation [19]. The vision feedback of task conduction is achieved by the RGB web camera and the ArUco maker board [20]. The control computer is in charge of torque control and the vision computer is in charge of video processing and virtual reality realization. By using these devices, the system can provide real-time information of online surgical tasks conduction and implement virtual reality tasks in vision interface for the tele-operator.

4. TASKS AND METHODOLOGY

4.1. Hands-on motion to locate the trocar position

For MIS, the robot should know where is the trocar position in the robot coordination frame. A simple hands-on motion mode is activated with $\boldsymbol{\tau_d} = \boldsymbol{D_h}(\dot{\boldsymbol{q}})$, where $\boldsymbol{D_h} \in R^{n\times n}$ is a hands-on damping matrix, to make the robot easy to stop when there is no extern force on the robot. The trocar position $\boldsymbol{P_t} \in R^3$ in Fig. 3 can be obtained by forward kinematic function $\boldsymbol{P_t} = \boldsymbol{X_p}(\boldsymbol{q})$.

4.2. Tele-operation surgical task implementation

As you can see from the tele-operated MIS scene in Fig. 4, the tool-tip trajectory and the RCM constraint must be simultaneously respected during the surgery. During the whole procedure, the tool-tip must go through the trocar position P_t, representing the RCM Constraint, where X_P and X_{P_d} are the actual and desired Cartesian position inside the abdomen, u_r is the rotation matrix from actual tip direction $\hat{u}$ and desired tip direction $\hat{u}_d$, and θ is the angle between $\hat{u}$ and $\hat{u}_d$. To achieve this objective, an online trajectory planning scheme is introduced. The operational coordinates $\boldsymbol{X} = [\boldsymbol{X_P},\boldsymbol{X_R}] \in R^m$ $(m = 6)$ are the actual tip pose, including the actual tool-tip position $\boldsymbol{X_P} = [x,y,z]$ and the actual tool orientation with Euler angle expressed by $\boldsymbol{X_R} = [\alpha,\beta,\gamma]$. $\boldsymbol{X_d} = [\boldsymbol{X_{P_d}},\boldsymbol{X_{R_d}}] \in R^m$ $(m = 6)$ is the desired tip pose, where $\boldsymbol{X_{P_d}} = [x_d,y_d,z_d]$ is the desired Cartesian position given by the master device and the desired orientation $\boldsymbol{X_{R_d}} = [\alpha_d,\beta_d,\gamma_d]$ is calculated based on $\boldsymbol{X_P}$ online in order to guarantee the tip going through the trocar position $\boldsymbol{P_t} \in [x_t,y_t,z_t]$ during the

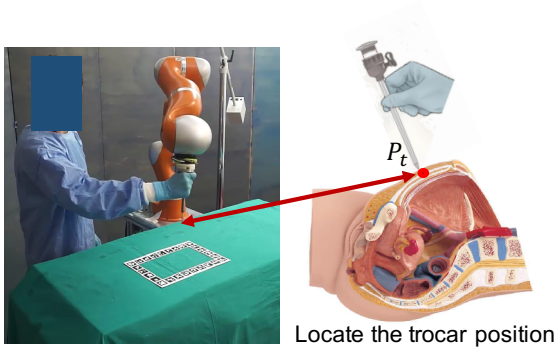

Fig. 3. Hands-on motion to locate the trocar position.

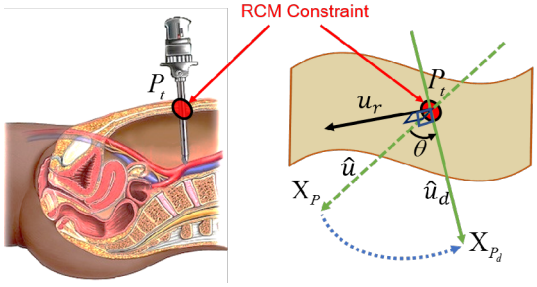

Fig. 4. Tele-operated MIS surgical scene.

movement, as follows:

The rotation angle θ (see Fig. 4) between the actual tool direction $\hat{u}$ and the desired tool direction $\hat{u}_d$ can be calculated as $\theta = \arctan \frac{\hat{u}_d \times \hat{u}}{\hat{u}_d \cdot \hat{u}}$. The unit vector describing a rotation axis $u_r = [u_x, u_y, u_z]$ from $\hat{u}$ to $\hat{u}_d$ is defined by $u_r = \frac{\hat{u}_d \times \hat{u}}{||\hat{u}_d \times \hat{u}||}$. A Skew-symmetric matrix is introduced by $\Gamma = [0, -u_z, u_y; u_z, 0, -u_x; -u_y, u_x, 0]$, and the desired orientation can be calculated using:

$$R_d = I + \Gamma sin(\theta) + 2\Gamma^2 \sin^2(\frac{\theta}{2}) \cdot R, \tag{8}$$

where R and R_d are the actual and desired rotation matrix, respectively. It is easy to get with Euler transformation from rotation matrix.

4.3. Redundancy collaboration in the null-space

The redundant robot can serve in a collaboration way with free motion in swivel angle during the surgery. It can provide more flexible workspace for the medical staff (assisting physicians, patient support) in the sharing workspace. When there is a collision between human and robot, the robot arm can be moved by hand in Fig. 5.

However, as it is mentioned in Fig. 1, not all the swivel angle is feasible for joint limitations. But the medical staff cannot know that, it is dangerous to move the swivel motion near the blocked swivel area, leading to a damage of the running system. Furthermore, the solution should also limit the swivel motion to avoid the known fixed physical objects or collision existing in the robot's workspace,

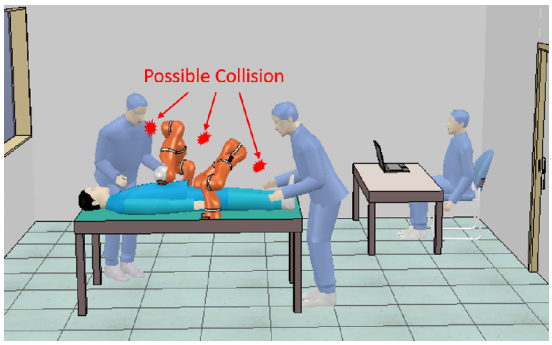

Fig. 5. Possible collision in the workspace.

for example, never touch the patient's body or other fixed medical devices, and never touch other robot arms in the sharing workspace. Hence, we can define a swivel motion constraint area $[\psi_{minf}, \psi_{maxf}]$, which is depend on the actual layout scene in the operating room. We assume that the proposed constraint area is always in the feasible swivel area $[\psi_{min}, \psi_{max}]$, and it is competent to avoid the fixed physical object in the sharing workspace. The medical staff can move the robot arm in the constraint area, but cannot go beyond the constraint to a dangerous area. A virtual force $F_\psi = u_{F_\psi} \cdot ||F_\psi||$ applied on the robot elbow is introduced to achieve the constraint of the swivel motion. The direction vector u_{F_ψ} of F_ψ is vertical of the robot arm plane (BSW), expressed by

$$u_{F_\psi} = sgn(\frac{\psi_{minf} + \psi_{maxf}}{2} - \psi) \cdot \frac{\vec{SE} \times \vec{EW}}{||\vec{SE} \times \vec{EW}||}. \tag{9}$$

The virtual force F_ψ is activated when the swivel motion is near the constraint boundary, compared as follows:

$$F_\psi = \begin{cases} u_{F_\psi} \cdot (k_\psi(\psi_{minf} + \rho - \psi) - d_\psi \dot{\psi}), & \psi < \psi_{minf}, \\ u_{F_\psi} \cdot (k_\psi(\psi_{maxf} - \rho - \psi) - d_\psi \dot{\psi}), & \psi > \psi_{maxf}, \\ 0, & [\psi_{minf}, \psi_{maxf}], \end{cases} \tag{10}$$

where $\rho \in R$ is a positive constant threshold value to avoid violation of the swivel constraint, $k_\psi, d_\psi \in R$ are the constant proportional coefficients.

Then the corresponding null-space projected torque $\boldsymbol{\tau}_N \in R^n$ generated from F_ψ is calculated as follows:

$$\boldsymbol{\tau_N} = \boldsymbol{N}(\boldsymbol{q}) \cdot (\boldsymbol{J_e^T F_\psi} - \hat{\boldsymbol{\tau}}_{\boldsymbol{EXT}}), \tag{11}$$

where $\boldsymbol{J}_e \in R^{3 \times n}$ is the Jacobian matrix between the robot base and the elbow, $\boldsymbol{N(q)} \in R^{n \times n}$ represents the null-space projector calculated using the inertia-weighted pseudo-inverse matrix $\boldsymbol{J(q)_M^+}$ [21], given by:

$$\boldsymbol{N}(\boldsymbol{q}) = \boldsymbol{I} - \boldsymbol{J}(\boldsymbol{q})^T (\boldsymbol{J}(\boldsymbol{q})_{\boldsymbol{M}}^+). \tag{12}$$

Fig. 6 shows the whole proposed control architecture. The candidate stability laypunov function for impedance control $\boldsymbol{\tau}_T$ has been certificated as stable in [18, 22]. When the $\boldsymbol{\tau}_N$ is applied, the stability is not influenced.

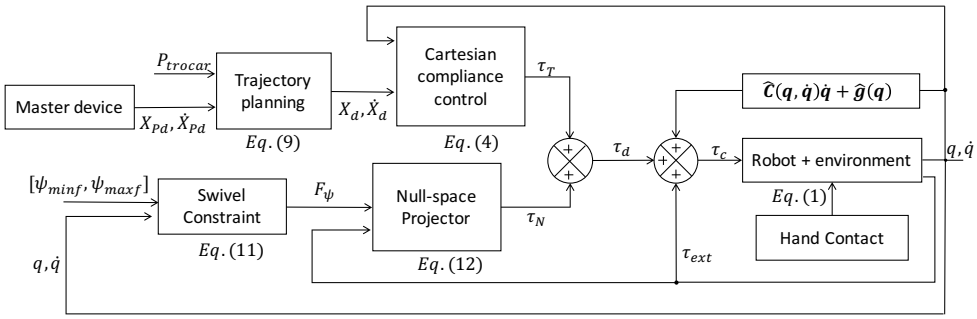

Fig. 6. Block diagram representing the proposed control architecture: The trajectory planning block is used to calculate the desired end-effector pose based on the Cartesian position without violation of the RCM constraint, cartesian compliance controller is to achieve the desired pose of the end effector, swivel constraint calculate the virtual force applied on the robot elbow, null-space projector is to map the virtual force to joints torque, robot and environment is robot arm dynamic model with extern disturbance, hand contact is with hand force on the robot arm.

5. EXPERIMENTAL PROTOCOL

The control system was developed with OROCOS (Open Robotic Control Software, http://www.orocos.org/) application in Ubuntu 12.04 with a real-time Xenomai-patched Linux kernel and ROS (Robot Operating System, http://www.ros.org/) kinetic in Ubuntu 16.04. In order to provide the user a visual interface of the developed tele-operation system without deterioration of the control frequency, ROS vision node and torque controller were executed on separate computers with UDP communication: the control loop was executed on the control computer and the vision ROS node was executed on the vision computer in Fig. 2. The camera in Fig. 2 provides the resolution with 1280×720 pixels in 8-bit per channel, delivering three basic color components of the images. It can achieve high-precision detection of the markers attached to the operating table based on the OpenCV ArUco library.

Two subjects were enrolled to participate to the experimental with the developed tele-operated MIS system. Desired virtual reality task paths were designed in vision interface for tele-operation tracking with different shapes: (I) Half ellipse curve, (II) Sine curve and (III) Triangle curve. The designed tasks were with the size around 8.0 cm $\times$ 15.0 cm on the horizonal plane, which is similar to the actual MIS task. The vision interface displayed the camera images, RCM constraint, desired task path, actual tip drawn paths on the display in Fig. 7.

In this experiment, two event-based steps were proposed start-up: pre-operative step and operative step. Before operation, the transformation from the task reference frame of ArUco board in Fig. 7 to the robot slave's base frame is estimated through a calibration process [20].

5.1. Operative procedure

5.1.1 pre-operative step

In this procedure, a hands-on motion control is activated for locating the trocar position in Fig. 3. Once the desired

Fig. 7. Operative step using the Kuka LWR 4+ robot.

trocar position has been set, the trocar constraint $\mathbf{P}_t$ will be plot with a blue point in the screen in Fig. 7.

5.1.2 operative step

Once the desired trocar position has been set, the tele-operation mode can be activated to conduct the surgical task. Desired surgical tracking tasks are shown with green curve in the screen, and the actual tip trajectory is plot in blue curve in Fig. 7. The tele-operator sits in front of the screen and control the robot tip with the master device try to follow the desired tracking tasks. The joint robot limitations are used to online calculate the feasible swivel motion range. The robot joint limitations were $[\pm 170, \pm 120, \pm 170, \pm 120, \pm 170, \pm 120, \pm 170]$ in degrees, given by the constructor. The communication frequency between the robot's controller and the control

Table 1. Experimental controller parameters.

Step	Controller	Parameters
Preoperative step	$\tau_d = D_h(\dot{q})$	$D_h = 5.2I_{7\times7}$
Operative step without constraint	$\tau_d = \tau_T$	$K_x = diag(3000,3000,3000, 300,300,300)$; $D_x = diag(30,30,30,3.5, 3.5,3.5)$;
Operative step with constraint	$\tau_d = \tau_T + \tau_N$	$K_x = diag(3000,3000,3000, 300,300,300)$; $D_x = diag(30,30,30,3.5, 3.5,3.5)$; $k_\psi = 150.0$; $d_\psi = 5.0$; $\rho = 0.12$

computer was 500Hz. The master device working rate is 1000Hz and the vision node working rate was set to 30Hz.

5.2. Experimental evaluation

To evaluate the proposed safety-enhanced collaborative strategy for the tele-operated MIS, we test it with two kinds of experiments: (A) Fixed end-effector pose, (B) Tele-operated tracking tasks. The comparison of the performance between the proposed safety-enhanced collaborative strategy and the method without safety constraint is conduct on fixed end-effector pose, ignoring the influence from difference in kinematic placement. Then the performance of the proposed safety-enhanced strategy is analyzed with tele-operation tracking tasks to validate if it is competent for the general tele-operated MIS tasks. The control parameter is shown in Talbe 1. The K_x is chosen by trial in this paper [23], and Dx is chosen based on the design procedure proposed in [18].

5.2.1 Experiment 1: Collaboration with fixed end-effector pose

The tele-operator didn't use the master device to control the robot, and the medical staff was command to try to move the robot elbow out of the set swivel constraint [-0.72,0.32]. 5 different fixed end-effector poses with different RCM constraints were tested and analyzed. For each fixed posed, the torque controller was switched between proposed strategy $\tau_d = \tau_T + \tau_N$ and the strategy without swivel constraint $\tau_d = \tau_T$ for comparison. The tests for each pose is repeated 10 times for each.

5.2.2 Experiment 2: Collaboration with tele-operated tracking tasks

The tele-operator use the master device to control the robot-tip to track the desired paths, and the medical staff was command to try to move the robot elbow out of the set swivel constraint [-0.72,0.32] at the same time. The torque controller is activated with the proposed safety-enhanced strategy $\tau_d = \tau_T + \tau_N$ during the whole procedure. The secondary experiment was evaluated with a continuous conduction of the three designed surgical task curves. It was repeated 6 times for each different RCM constraints. For both experiments, RCM constraint P_t , desired Cartesian position $X_{P_d} = [x_d, y_d, z_d]$ of the end effector, actual end-effector Cartesian position $X_P = [x, y, z]$ of the end effector, and the swivel angle ψ of the robot arm were collected. The Cartesian error $E_x = ||x - x_d||, E_y = ||y - y_d||, E_z = ||z - z_d||$, and the RCM constraint error E_{P_t} is computed for comparison or analyzed, where $E_{p_t} = ||(P_t - X_p) \times \hat{u}_c||$ and $\hat{u}_c$ is actual tip unit direction vector. The root means square error (RMSE) for Cartesian accuracy λ_{X_p} and RCM constraint λ_P during each experiment procedure were calculated separately to verify the performance of the proposed strategy:

$$\lambda_{X_p} = \sqrt{\frac{\sum_{i=1}^{n} ||X_{P_i} - X_{P_{di}}||^2}{n}}, \tag{13}$$

$$\lambda_P = \sqrt{\frac{\sum_{i=1}^{n} ||E_{P_i i}||^2}{n}}, \tag{14}$$

where $X_{P_{di}}$ and X_{P_i} are the ith desired and actual Cartesian position, respectively; $E_{P_i i}$ is the ith RCM constraint error.

5.3. Experimental results

5.3.1 Results with fixed Cartesian position

Fig. 8(a) shows the swivel motion of the experiment on the fixed pose 1 in Table 2. Firstly, the safety-enhanced strategy was applied on the swivel motion, it is easy to see that when it is near or want to pass through the swivel boundary , the virtual force will be activated to limit the swivel motion. And then the constraint on swivel motion is canceled, it is free to move the swivel motion without any constraint. The corresponding virtual force applied on the elbow is shown in Fig. 8(b) during the whole procedure, and the corresponding Cartesian error around each axis is shown in Fig. 8(c). Since the uncertain disturbance and the calibration error of the robot dynamical parameters exist during the human-robot interaction and we didn't utilize adaptive nonlinear controller, the Cartesian position error does not converge to zero. The RCM constraint and Cartesian error were compared in Table 2.

5.3.2 Results with tele-operated tracking tasks

Fig. 9(a) shows the swivel motion of the tele-operated MIS manipulator with three tracking tasks. The safety-enhanced strategy was applied on the controller during the whole procedure, it is easy to see that when it is near or want to pass through the swivel boundary , the virtual force will be activated to limit the swivel motion in Fig. 9(b). And the corresponding Cartesian error around each axis of the same procedure is shown in Fig. 9(c). Since the uncertain disturbance and the calibration error of the robot dynamical parameters exist during the human-robot interaction and we didn't utilize adaptive nonlinear

Table 2. Performance evaluation with fixed target poses.

		Safety-enhanced collaborative strategy $\tau_d = \tau_T + \tau_N$		Collaborative strategy without constraint $\tau_d = \tau_T$	
Fixed end-effector Pose	Feasible swivel angle $[\psi_{min}, \psi_{max}]$	Cartesian accuracy error $\lambda_{X_p}(m)$	RCM constraint error $\lambda_P(m)$	Cartesian accuracy error $\lambda_{X_p}(m)$	RCM constraint error $\lambda_P(m)$
Pose 1	[-2.47, 2.88]	0.0016 ± 0.0003	0.0043 ± 0.0002	0.0017 ± 0.0004	0.0046 ± 0.0003
Pose 2	[-1.795, 2.97]	0.0017 ± 0.0004	0.0040 ± 0.0005	0.0019 ± 0.0003	0.0044 ± 0.0003
Pose 3	[-1.785, 2.971]	0.0014 ± 0.0003	0.0013 ± 0.0004	0.0013 ± 0.0004	0.0014 ± 0.0002
Pose 4	[-2.562, 2.561]	0.0014 ± 0.0004	0.0025 ± 0.0007	0.0020 ± 0.0003	0.0026 ± 0.0004
Pose 5	[-2.283, 2.961]	0.0020 ± 0.0003	0.0032 ± 0.0004	0.0020 ± 0.0003	0.0030 ± 0.0004

The performance of the corresponding Cartesian accuracy error and RCM constraint error were analyzed for comparison with 5 different fixed end-effector pose, Pose 1-5: $[-0.4636$ m, 0.3800 m, 0.1124 m, -2.9497 rad, 0.0360 rad, 0.3618 rad$]$, $[-0.3934$ m, 0.3526 m, 0.1225 m, -2.7560 rad, 0.0420 rad, 0.2425 rad$]$, $[-0.4123$ m, 0.3844 m, 0.1422 m, -2.3445 rad, 0.0540 rad, 0.3312 rad$]$, $[-0.5332$ m, 0.4200 m, 0.1023 m, -2.7897 rad, 0.0422 rad, 0.3511 rad$]$, $[-0.4798$ m, 0.3524 m, 0.1326 m, -2.9661 rad, 0.0355 rad, 0.4500 rad$]$. The error in the table is mean value of the total 10 times testing.

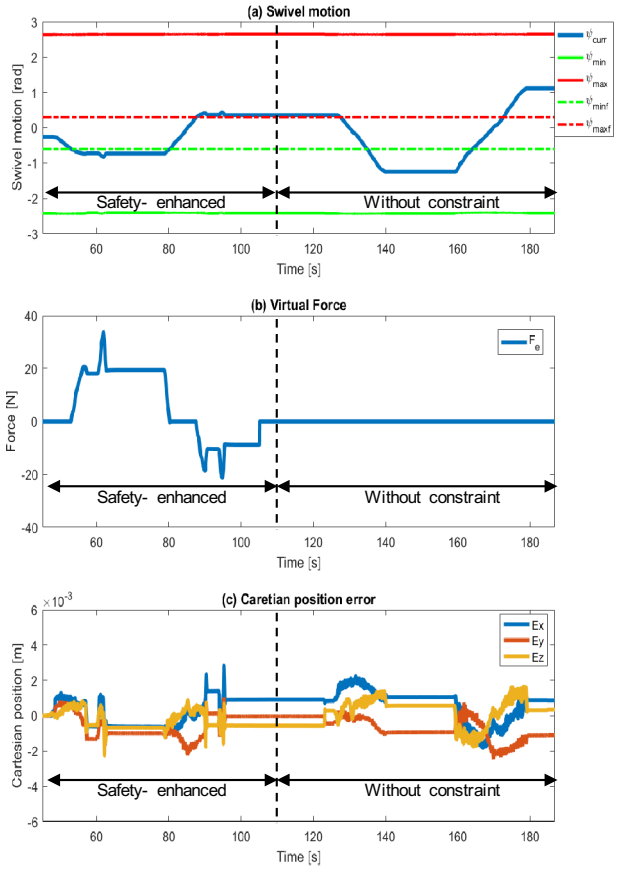

Fig. 8. Experiments on the fixed pose 1.

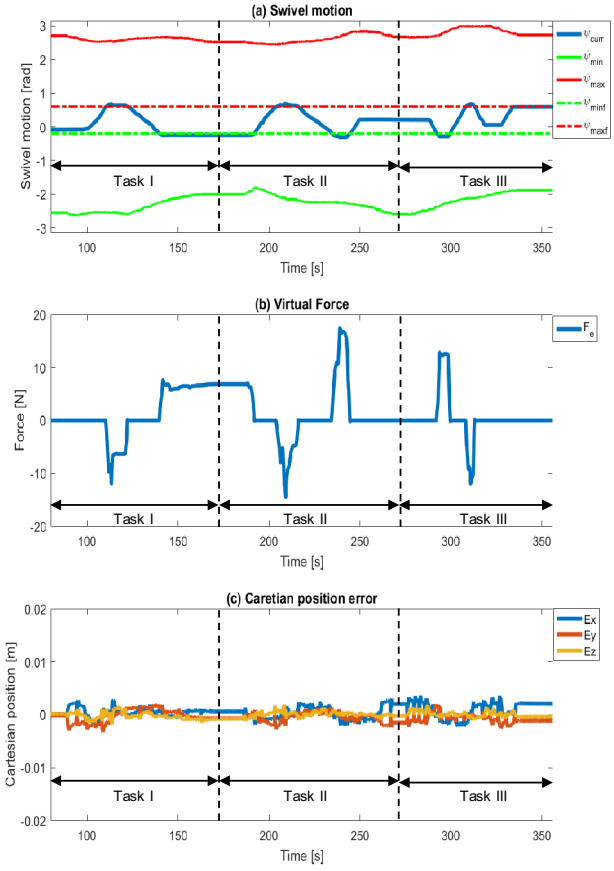

Fig. 9. Experiments on the tele-operation tracking tasks.

controller, the Cartesian position error does not converge to zero. The experiments are conducted with three different RCM constraints and its corresponding RCM constraint error were analyzed in Table 3.

6. DISCUSSION AND CONCLUSION

Finally, it can be included form the results that the proposed strategy can achieve safety constraint on the swivel motion without obvious influence on the Cartesian accuracy and RCM constraint. From Table 2, the proposed general collaborative framework is competent for the general tele-operated MIS tasks. This paper developed a collaborative framework for MIS using a 7-DoF torque controlled redundant robot. Experimental evaluations were conducted with virtual surgical tasks to validate the performance. The robot's elbow can be moved freely within the

Table 3. Performance evaluation of online tracking tasks.

RCM point	Cartesian accuracy error $\lambda_{X_p}(m)$	RCM constraint error $\lambda_P(m)$
P_{t1}	0.0018 ± 0.0003	0.0027 ± 0.0005
P_{t2}	0.0019 ± 0.0003	0.0032 ± 0.0004
P_{t3}	0.0016 ± 0.0004	0.0025 ± 0.0007

Tele-operation tracking was conduct with the three tracking tasks. The root-mean-square error (RMSE) of Cartesian accuracy and RCM constraint were calculated for each task.

constrained swivel area by hand in collaborative way without a degradation of the quality of the surgical task. The developed impedance control strategy can also be applied in a wide variety of anthropomorphic robot arms with similar structure not only for MIS surgery, also for industry with similar application scene. However, in this paper, we choose an assumed safe swivel motion range based on feasible swivel range, which is within the joints limitations. It is necessary to achieve the online avoidance of the joints limitations in the future. The developed scheme was only evaluated on the virtual surgical tasks. In future, the surgical tasks in virtual reality will be developed with dynamic model to simulate real object contact on surgical tool-tip. Disturbance observer based adaptive neural network [24–26] or fuzzy adaptive controller [27] will be adopted to coverage the error of the end-effector. With the popularity of surgical robots in the operating room, it can be expected to see more research efforts expended in this field.

REFERENCES

[1] Z. Li, J. Feiling, H. Ren, and H. Yu, "A novel teleoperated flexible robot targeted for minimally invasive robotic surgery," *Engineering*, vol. 1, no. 1, pp. 73-78, 2015.

[2] A. R. Lanfranco, A. E. Castellanos, J. P. Desai, and W. C. Meyers, "Robotic surgery: a current perspective," *Annals of surgery*, vol. 239, no. 1, p. 14, 2004.

[3] M. Tavakoli, R. V. Patel, and M. Moallem, "A force reflective master-slave system for minimally invasive surgery," *Proceedings of IEEE/RSJ International Conference on Intelligent Robots and Systems (IROS 2003)*, IEEE, vol. 4, pp. 3077-3082, 2003.

[4] G. Rateni, M. Cianchetti, G. Ciuti, A. Menciassi, and C. Laschi, "Design and development of a soft robotic gripper for manipulation in minimally invasive surgery: a proof of concept," *Meccanica*, vol. 50, no. 11, pp. 2855-2863, 2015.

[5] N. Enayati, E. De Momi, and G. Ferrigno, "A quaternion-based unscented kalman filter for robust optical/inertial motion tracking in computer-assisted surgery," *IEEE Transactions on Instrumentation and Measurement*, vol. 64, no. 8, pp. 2291-2301, 2015.

[6] H. Su, G. Ferrigno, and E. De Momi, "Event-based adaptive control of 7-dof serial robot for teleoperated mis," *Proc. of 6th National Congress of Bioengineering*, Politecnico di Milano, 2018.

[7] H. Su, J. Sandoval, M. R. Makhdoomi, G. Ferrigno, and E. De Momi, "Safety-enhanced human-robot interaction control of redundant robot for teleoperated minimally invasive surgery," *Proc. of International Conference on Robotics and Automation*, pp. 6611-6616, 2018.

[8] N. Aghakhani, M. Geravand, N. Shahriari, M. Vendittelli, and G. Oriolo, "Task control with remote center of motion constraint for minimally invasive robotic surgery," *Proc. IEEE International Conference on of Robotics and Automation (ICRA)*, IEEE, pp. 5807-5812, 2013.

[9] H. Su, G. Ferrigno, and E. De Momi, "Adaptive decoupling control of a serial redundant robot for teleoperated minimally invasive surgery," *Proc. of IEEE ICRA Workshop on Supervised Autonomy in Surgical Robotics*, 2018.

[10] J. Baillieul, "Avoiding obstacles and resolving kinematic redundancy," *Proc. IEEE International Conference on of Robotics and Automation*, IEEE, vol. 3, pp. 1698-1704, 1986.

[11] L. Jin, S. Li, H. M. La, and X. Luo, "Manipulability optimization of redundant manipulators using dynamic neural networks," *IEEE Transactions on Industrial Electronics*, 2017.

[12] T. Beyl, P. Nicolai, J. Raczkowsky, H. Worn, M. D. Comparetti, and E. De Momi, "Multi kinect people detection for intuitive and safe human robot cooperation in the operating room," *Proc. 16th International Conference on of Advanced Robotics (ICAR)*, IEEE, pp. 1-6, 2013.

[13] M. Shimizu, H. Kakuya, W.-K. Yoon, K. Kitagaki, and K. Kosuge, "Analytical inverse kinematic computation for 7-dof redundant manipulators with joint limits and its application to redundancy resolution," *IEEE Transactions on Robotics*, vol. 24, no. 5, pp. 1131-1142, 2008.

[14] M. D. Comparetti, E. Beretta, M. Kunze, E. De Momi, J. Raczkowsky, and G. Ferrigno, "Event-based device-behavior switching in surgical human-robot interaction," *Proc. IEEE International Conference on of Robotics and Automation (ICRA)*, IEEE, pp. 1877-1882, 2014.

[15] Y. Pan, Y. Liu, B. Xu, and H. Yu, "Hybrid feedback feedforward: an efficient design of adaptive neural network control," *Neural Networks*, vol. 76, pp. 122-134, 2016.

[16] C. Yang, J. Luo, Y. Pan, Z. Liu, and C. Su, "Personalized variable gain control with tremor attenuation for robot teleoperation," *IEEE Transactions on Systems, Man, and Cybernetics: Systems*, vol. 48, no. 10, pp. 1759-1770, Oct. 2018.

[17] G. Schreiber, A. Stemmer, and R. Bischoff, "The fast research interface for the kuka lightweight robot," *Proc. of IEEE Workshop on Innovative Robot Control Architectures for Demanding (Research) Applications How to Modify and Enhance Commercial Controllers (ICRA 2010)*, pp. 15-21, 2010.

[18] A. Dietrich, T. Wimbock, A. Albu-Schaffer, and G. Hirzinger, "Integration of reactive, torque-based self-collision avoidance into a task hierarchy," *IEEE Transactions on Robotics*, vol. 28, no. 6, pp. 1278-1293, 2012.

[19] N. ENAYATI, "Adaptive shared-control in surgical robotics," 2017.

[20] S. Garrido-Jurado, R. Muñoz-Salinas, F. J. Madrid-Cuevas, and M. J. Marín-Jiménez, "Automatic generation and detection of highly reliable fiducial markers under occlusion," *Pattern Recognition*, vol. 47, no. 6, pp. 2280-2292, 2014.

[21] O. Khatib, "A unified approach for motion and force control of robot manipulators: the operational space formulation," *IEEE Journal on Robotics and Automation*, vol. 3, no. 1, pp. 43-53, 1987.

[22] C. Ott, "Cartesian impedance control: The rigid body case," *Cartesian Impedance Control of Redundant and Flexible-Joint Robots*, Springer, pp. 29-44, 2008.

[23] A. Albu-Schaffer, C. Ott, U. Frese, and G. Hirzinger, "Cartesian impedance control of redundant robots: Recent results with the dlr-light-weight-arms," *Proc. of IEEE International Conference on Robotics and Automation (ICRA'03)*, IEEE, vol. 3, pp. 3704-3709, 2003.

[24] Y. Pan, Y. Liu, and H. Yu, "Simplified adaptive neural control of strict-feedback nonlinear systems," *Neurocomputing*, vol. 159, pp. 251-256, 2015.

[25] Y. Pan and H. Yu, "Biomimetic hybrid feedback feedforward neural-network learning control," *IEEE Transactions on Neural Networks and Learning Systems*, vol. 28, no. 6, pp. 1481-1487, 2017.

[26] C. Yang, Y. Jiang, Z. Li, W. He, and C.-Y. Su, "Neural control of bimanual robots with guaranteed global stability and motion precision," *IEEE Transactions on Industrial Informatics*, vol. 13, no. 3, pp. 1162-1171, 2017.

[27] Z. Li, C.-Y. Su, G. Li, and H. Su, "Fuzzy approximation-based adaptive backstepping control of an exoskeleton for human upper limbs," *IEEE Transactions on Fuzzy Systems*, vol. 23, no. 3, pp. 555-566, 2015.

Hang Su received the M.Sc. degree in Control theory and control engineering in South China University of Technology, Guangzhou, China. He is pursuing a Ph.D. degree as a member of the Medical and Robotic Surgery group (NEARLab) in Politecnico di Milano, Milano, Italy, working on control of surgical robots.

Juan Sandoval is currently an Assistant Professor at PPRIME Institute, University of Poitiers, France. He received his Ph.D. degree on robotics from the University of Orleans, France, in 2017. He also obtained a Mechatronics Engineering degree from the National University of Colombia and a Master's degree from the National School of Engineering ENIVL, France (2012).

Pierre Vieyres received his M.Sc. in Electrical engineering from University College London (UK), and his Ph.D. degree in 1990 in biomedical engineering from the University of Tours (France). In 1992, he joined the University of Orleans (France) he is a full Professor in the Robotics Team of PRISME laboratory.

Gérard Poisson is a Professor at the University of Orleans (France) and a researcher at PRISME Laboratory. He obtained the French Agregation of Mechanics in 1980 and a Ph.D. in robotics at Orleans University in 1994. He is currently the director of the Bourges Institute of Technology (IUT) and deputy director of PRISME Laboratory.

Giancarlo Ferrigno received the M.Sc. degree in electrical engineering and the Ph.D. degree in bioengineering from the Politecnico di Milano, Milan, Italy. He is a Full Professor of Medical Robotics and the Founder of the Neuroengineering and Medical Robotics Laboratory with the Department of Electronics, Information and Bioengineering, Politecnico di Milano.

Elena De Momi received her M.Sc. and Ph.D. degrees in biomedical engineering from the Politecnico di Milano, Milan, Italy. She is currently an Assistant Professor in the Department of Electronics, Information, and Bioengineering, Politecnico di Milano.